Plasma-Activated Fenton Chemistry for Acid Blue 9 dye removal: Kinetics, physicochemical dynamics, and G_{50} optimization

J. Vergara[a], E. Gutiérrez[a], C. Torres[b,*], E. Montiel[b], B. Bazaldua[c], A. Gómez[d], P. G. Reyes[d], and H. Martínez[e]

[a]*Laboratorio de Ingeniería Ambiental, Facultad de Ciencias Químicas e Ingeniería, Universidad Autónoma del Estado de Morelos, Av. Universidad 1001, Chamilpa, Cuernavaca, Morelos, 62210, México.*

[b]*Laboratorio de Análisis y Sustentabilidad Ambiental, Escuela de Estudios Superiores de Xalostoc, Universidad Autónoma del Estado de Morelos, Av. Nicolás Bravo S/N, Ayala, Morelos, 62715, México.*

[c]*Escuela de Estudios Superiores de Atlatlahucan, Universidad Autónoma del Estado de Morelos, Galeana 146, San Antonio, Atlatlahucan, Morelos, 62840, México.*

[d]*Laboratorio de Física Avanzada, Facultad de Ciencias, Universidad Autónoma del Estado de México, Instituto Literario No. 100 Col. Centro, Toluca, Estado de México, 50000, México.*

[e]*Laboratorio de Espectroscopia, Instituto de Ciencias Físicas, Universidad Nacional Autónoma de México, Apartado Postal 48-3, Cuernavaca, Morelos, 62251, México.*

[*]*e-mail: cesar.torres@uaem.mx*

Received 22 june 2026; accepted 7 july 2026

Industrial effluents containing synthetic dyes represent one of the most persistent sources of surface water contamination, largely because conventional treatment processes fail to achieve their complete removal. In this work, we evaluated the degradation efficiency of a Non-Thermal Atmospheric-Pressure Plasma (NTAPP) system toward Acid Blue 9 (AB9) dye, using $FeSO_4$ as a catalytic additive at concentrations ranging from 0.2 to 1.0 mM. Degradation was monitored by UV-Vis absorbance at 630 nm, and solution physicochemical parameters pH, electrical conductivity, salinity, total dissolved solids (TDS), and bulk solution temperature were recorded throughout treatment. After 30 minutes of plasma exposure, near complete decolorization was achieved, with optimal catalytic performance observed at 0.6 mM $FeSO_4$. The enhanced degradation at this concentration is consistent with a Fenton-type mechanism, in which Fe^{2+} ions react with plasma-generated H_2O_2 to produce additional ·OH radicals. TOC analysis confirmed a dye mineralization efficiency exceeding 90%. These results demonstrate the potential of catalytically intensified NTAPP as an effective strategy for the treatment of dye contaminated water.

Keywords: Non-thermal plasma; AB9; triarylmethane dye.

DOI: https://doi.org/10.31349/RevMexFis.72.061501

1. Introduction

Textile industry effluents are among the most chemically complex wastewaters generated by any industrial sector. A recurring problem is the discharge of synthetic dyes that resist conventional biological and physicochemical treatment Acid Blue 9 (AB9) being a well-documented example [1]. During fabric dyeing, an estimated 10–15% of the dye applied fails to bind to the fiber substrate; this unbound fraction is flushed out in process wastewater and eventually reaches surface water bodies, where its persistence becomes an ecological liability [2].

What makes synthetic dyes particularly problematic is not just their color. These compounds are designed to resist fading, which means they also resist environmental degradation. In aquatic systems, their high solubility keeps them in the water column rather than settling out, while their structural stability allows them to persist for extended periods [3]. Over time, bioaccumulation through the food chain becomes a concern, and some dyes break down into transformation products that are more acutely toxic than the original molecule [4]. The ecological consequences are tangible: dye-contaminated water absorbs and scatters light, suppressing photosynthesis in aquatic plants and disrupting the base of freshwater food webs [1,5].

Beyond the ecosystem, the human health implications are serious. AB9, specifically, has been classified as a potentially carcinogenic and mutagenic compound. Subcutaneous administration in rat models produced carcinogenic effects, and oral ingestion was associated with a higher incidence of renal tumors [1,6]. Given that human exposure can occur through consumption of contaminated drinking water or trophic transfer, treatment strategies that fully mineralize this dye, rather than simply transferring it to another phase, are not optional; they are necessary [6,7].

Dye removal from wastewater is therefore both an environmental and a public health imperative. It also bears directly on freshwater availability: in regions facing water scarcity, the ability to treat and reuse industrial effluents could substantially reduce demand on freshwater reserves. Conventional methods of biological treatment, coagulation, and adsorption have well-known limitations when applied to

recalcitrant dyes. They either fail to achieve complete removal or generate secondary waste streams that require further management [8,9].

Advanced Oxidation Processes (AOPs) address these limitations through a fundamentally different mechanism: the in-situ generation of hydroxyl radicals (·OH), which are among the most powerful oxidizing agents known in aqueous chemistry [10]. Unlike biological processes, ·OH radicals do not select their targets; they attack aromatic rings, conjugated bonds, and other organic structures indiscriminately, driving mineralization to CO_2, H_2O, and inorganic salts [11]. This makes AOPs well suited for compounds that have specifically evolved, so to speak, to resist biological attack.

Among the AOP family, non-thermal atmospheric-pressure plasma (NTAPP) occupies a distinctive position. Rather than relying on a single reactive species, plasma discharge simultaneously generates a cocktail of reactive oxygen and nitrogen species (RONS), including ·OH, O_3, H_2O_2, and UV photons, without consuming chemical reagents or producing hazardous byproducts [12,13]. The system operates at atmospheric pressure and can be switched on and off on demand, which simplifies reactor design and operational control relative to other AOP configurations. In AOPs, the mineralization of contaminants occurs in successive stages. The first stage involves the generation of reactive species (O_3, H_2O_2), primarily the hydroxyl radical (·OH). This pathway begins with the dissociation of water molecules by energetic electrons generated during plasma discharge:

$$e^- + H_2O \rightarrow \cdot OH + H^\bullet + e^-. \quad (1)$$

The ·OH radicals produced in Eq. (1) can subsequently recombine in the bulk solution to form hydrogen peroxide:

$$\cdot OH + \cdot OH \rightarrow H_2O_2. \quad (2)$$

This accumulated H_2O_2 becomes a secondary source of ·OH when a ferrous iron catalyst is present. The addition of $FeSO_4$ triggers a Fenton-type reaction that regenerates radicals from the peroxide pool:

$$Fe^{2+} + H_2O_2 \rightarrow Fe^{3+} + \cdot OH + OH^-. \quad (3)$$

Once these reactive species are generated, oxidative attack occurs on the contaminants (AB9) present in the medium. The ·OH radical reacts non-specifically with the contaminant molecule, initiating oxidation and destabilizing its chemical structure. The oxidation of AB9 is primarily due to highly reactive species such as the hydroxyls (·OH) generated during discharge, leading to the formation of intermediate compounds and partial mineralization products [11,12,14], as represented in Eqs. (4) and (5):

$$AB9 + \cdot OH \rightarrow \text{oxidation intermediate}. \quad (4)$$

Finally, these unstable structures fragment into intermediates, which ultimately break down into their most basic and harmless mineral components:

$$\text{oxidation intermediate} \rightarrow CO_2 + H_2O + \text{inorganic ion}. \quad (5)$$

This coupling between plasma-generated H_2O_2 and Fe^{2+}-driven Fenton chemistry creates a synergistic amplification of the oxidative capacity of the system [14]. The resulting radical flux attacks the chromophoric structure of AB9, specifically the conjugated π-system and the aromatic rings associated with its triarylmethane backbone. The species preferentially attack the central carbon atom and the aromatic rings of the AB9 molecule, which constitute its chromophore system. This attack leads to the disruption of the triarylmethane structure and promotes the breaking of conjugated π bonds and the opening of the aromatic rings, resulting in the formation of several low molecular weight organic intermediates. This leads to progressive decolorization and, ultimately, mineralization.

AB9 (Brilliant Blue FCF; MW = 792.86 g/mol; CAS 3844-45-9; $C_{37}H_{34}N_2Na_2O_9S_3$; CI 42090) is an appropriate model contaminant for this study for several reasons. It is widely used across food, cosmetic, pharmaceutical, and textile applications [15,16], which ensures its practical relevance. Its well defined absorption maximum at 630 nm allows straightforward spectrophotometric monitoring. And its documented toxicological profile, including carcinogenicity in animal models, makes its effective removal a meaningful benchmark for treatment performance.

In this work, we evaluate the efficiency of an NTAPP system for the degradation of AB9, using $FeSO_4$ as a catalytic additive at concentrations ranging from 0.2 to 1.0 mM. The specific objective is to identify the optimal catalyst concentration and to characterize the physicochemical changes in the treated solution throughout the plasma exposure period.

2. Material and methods

A batch reactor (Fig. 1) was used to generate a corona discharge at the surface of the liquid sample. The discharge was generated by a DC power supply (Advanced Energy, PNCL PLUS+) operating at a frequency of 5 kHz and a power input of 40 W.

The following physicochemical parameters were monitored throughout the treatment: pH, electrical conductivity, total dissolved solids (TDS), salinity, and bulk solution temperature, using a Hach HQ40d multiparameter meter. UV-Vis absorbance of the treated solutions was measured at discrete $FeSO_4$ concentrations ranging from 0.2 to 1.0 mM (in

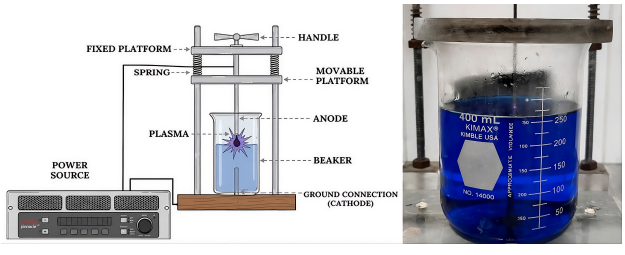


FIGURE 1. Batch reactor used for plasma treatment of AB9 dye solutions.

0.2 mM increments) using a Hach DR3900 spectrophotometer. The maximum absorption wavelength (λ_{max}) of AB9 was determined to be 630 nm, which was used as the analytical wavelength for all absorbance measurements.

Total organic carbon (TOC) was determined using the Hach TNT plus low-range vial method.

2.1. Reactor configuration

The plasma generation reactor consists of a beaker containing two tungsten electrodes. The anode is positioned on the surface of the beaker holding the sample, and the cathode is placed on the surface of the sample to be treated (2 mm). The beaker has an acrylic lid, and the cathode passes through the lid via a 3 mm diameter hole. The beaker is placed inside an acrylic container.

2.2. Sample preparation

Samples were prepared with a concentration of 0.1 mM in a volume of 250 mL. For this purpose, 0.0198 g of Acid Blue 9 dye was weighed. The mass was transferred to a 250 mL beaker containing 100 mL of distilled water, stirring constantly for 5 minutes. Subsequently, the solution was transferred to a 250 mL volumetric flask where the catalyst was added using a 5 mL pipette with the aid of a precision pipette, and the flask was filled to the mark with distilled water. The degradation of AB9 dye was investigated at an initial dye concentration of 0.1 mM, varying volumes of the catalyst stock solution were added to each sample, which was subsequently diluted to a total volume of 250 mL. Plasma treatment was applied for 30 minutes in all experiments. The catalyst was prepared at a concentration of 50 mM ($FeSO_4$) + 1.0 M (H_2SO_4). For its preparation, 3.47 g of ferrous sulfate were weighed and 1.4 mL of H_2SO_4 were added to a 250 mL beaker containing 100 mL of distilled water. The solution was stirred for 30 minutes. It was then transferred to a 250 mL volumetric flask and diluted to the mark with distilled water. Different volumes of the catalyst were added to the solution, from 1 mL (0.2 mM) up to 5 mL (1.0 mM). At the end of each treatment, the samples were stored in 250 mL amber glass bottles, in order to avoid any type of contamination; each experiment was performed 5 times.

3. Results

3.1. Decolorization of AB9 by Plasma Treatment

Figure 2 illustrates the progressive decolorization of AB9 dye solutions over increasing plasma treatment times. AB9 belongs to the triarylmethane class of synthetic dyes, whose intense blue coloration originates from a conjugated π-electron system centered on a central sp^3 carbon bonded to three aromatic rings. As treatment progressed, the optical absorbance at 630 nm declined steadily until the solution became virtually colorless after 30 minutes of plasma exposure. This

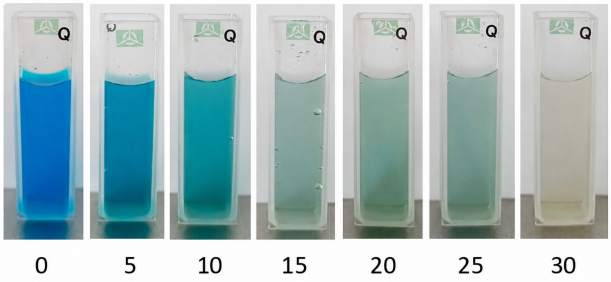


FIGURE 2. Progressive decolorization of AB9 dye solution as a function of plasma treatment time.

progressive loss of color reflects the disruption of the chromophore system through cleavage of the conjugated π-bonds responsible for visible-light absorption. The reduction in the characteristic absorption band at 630 nm confirms that AB9 degradation is driven by the RONS generated during plasma discharge, principally ·OH, O_3, and H_2O_2, which collectively promote the oxidative breakdown of the dye molecule [17,18].

3.2. Effect of $FeSO_4$ Concentration on Degradation Efficiency

Figure 3 present the UV-Vis absorbance spectra of AB9 at each $FeSO_4$ concentration tested [3a) to 3e)]. In all cases, the absorbance band at $\lambda_{max} = 630$ nm decreased progressively with treatment time, confirming that plasma-driven oxidation was active across the entire concentration range studied. The rate and extent of decolorization varied markedly with catalyst dosage, however, revealing a well-defined optimum. At the lowest catalyst concentration tested, 0.2 mM $FeSO_4$ [Fig. 3a)], absorbance decreased only modestly over 30 minutes and complete decolorization was not achieved. The limited performance is consistent with insufficient Fe^{2+} availability: with little Fe^{2+} present, decomposition of plasma-produced H_2O_2 into ·OH radicals is constrained, and the overall oxidative capacity remains below the threshold required for complete chromophore destruction. Increasing the catalyst concentration to 0.4 mM $FeSO_4$ [Fig. 3b)] produced a noticeably greater reduction in absorbance, indicating that higher Fe^{2+} availability translated into more effective ·OH generation via H_2O_2 decomposition. Nevertheless, decolorization remained incomplete at 30 minutes [19]. At 0.6 mM $FeSO_4$ [Fig. 3c)], representing the optimal condition, the most pronounced decline in band intensity was observed. By 30 minutes, the absorption band at 630 nm had disappeared entirely, indicating near complete degradation of the AB9 chromophore. This result demonstrates that 0.6 mM is the optimal catalyst dosage, at which Fenton-type coupling between Fe^{2+} and plasma-generated H_2O_2 achieves maximum ·OH production [19]. At 0.8 mM $FeSO_4$ [Fig. 3d)], the decolorization rate was lower than at the optimum, and a residual absorption band persisted after 30 minutes. This decline is attributed to the radical scavenging effect of excess Fe^{2+}: at supraoptimal concentrations, Fe^{2+} competes with organic substrates for ·OH radicals through the reaction

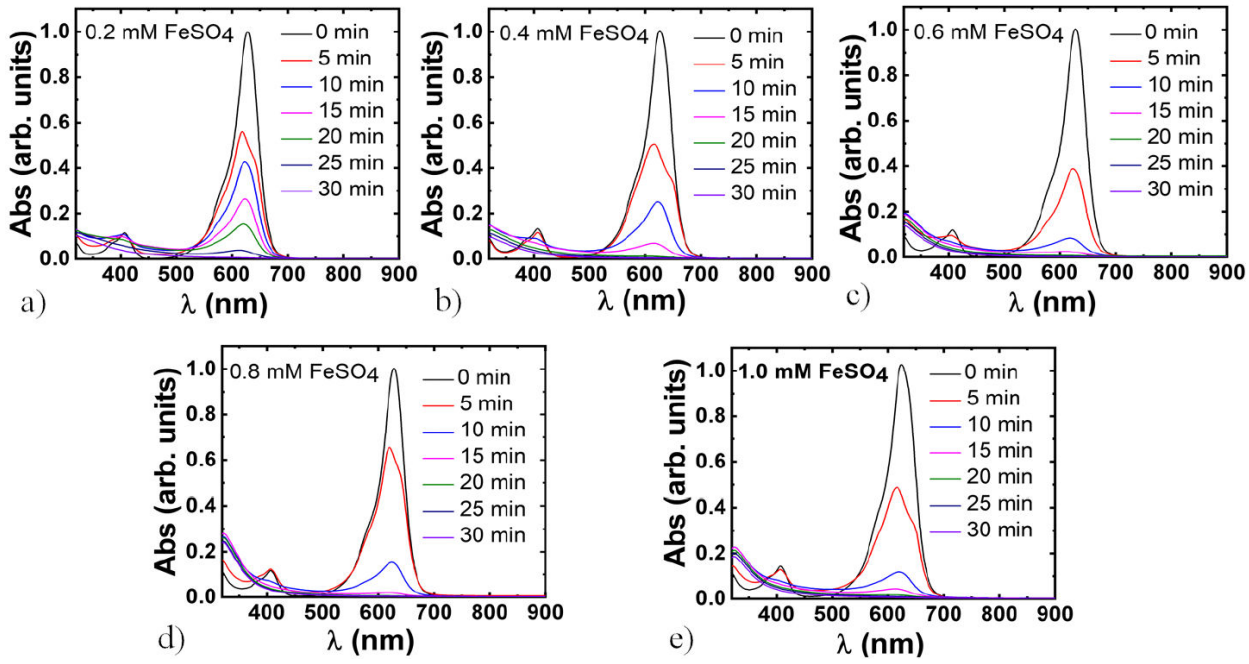


FIGURE 3. UV-Vis absorbance spectra of AB9 during plasma treatment at $FeSO_4$ concentrations of (A) 0.2 to (E) 1.0 mM.

$Fe^{2+} + \cdot OH \rightarrow Fe^{3+} + OH^-$ [18]. The highest catalyst concentration,1.0 mM $FeSO_4$ [Fig. 3e)], yielded the poorest decolorization among the supraoptimal conditions. The overabundance of Fe^{2+} intensifies radical scavenging competition, suppressing ·OH availability and limiting oxidative attack on the dye. These results collectively confirm that the relationship between $FeSO_4$ concentration and degradation efficiency is non-monotonic, with a well-defined maximum at 0.6 mM.

3.3. Mineralization and reaction kinetics

The normalized TOC/TOC_0 ratio as a function of plasma exposure time is shown in Fig. 4. In all cases, TOC/TOC_0 decreased progressively with treatment time, confirming actual mineralization of AB9. The steepest decline occurred during the initial phase, particularly at 0.6 mM $FeSO_4$. As treatment proceeded, the rate of TOC removal slowed characteristic of AOPs systems where recalcitrant intermediates exhibit lower reactivity toward ·OH than the parent compound [18]. At 0.6 mM $FeSO_4$, mineralization efficiency exceeded 90% within 30 minutes. Decolorization followed an apparent pseudo-first-order model, with rate constants of: $\kappa = 0.0895$ min^{-1} (0.2 mM), 0.1499 min^{-1} (0.4 mM), 0.2093 min^{-1} (0.6 mM), 0.1371 min^{-1} (0.8 mM), and 0.1202 min^{-1} (1.0 mM). The maximum rate constant at 0.6 mM is consistent with the optimal Fenton-type catalytic condition.

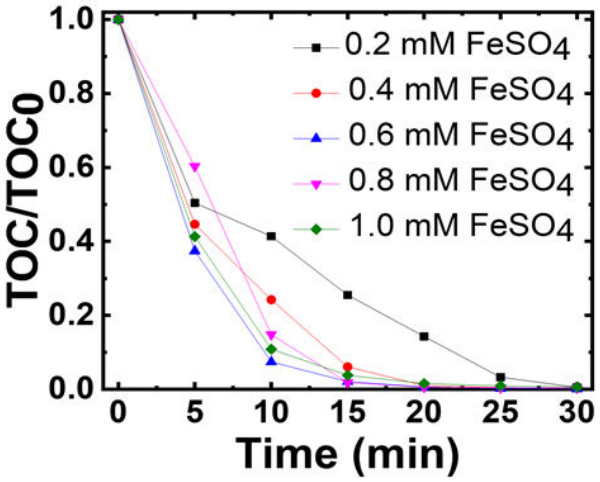


FIGURE 4. Normalized TOC/TOC_0 profiles as a function of plasma exposure time.

3.4. Physicochemical Evolution of the Treated Solution

The bulk solution temperature rose from approximately 22°C to 45°C over the 30-minute treatment [Fig. 5a)]. The most rapid increase occurred during the first 10–15 minutes, after which the system approached quasi-thermal equilibrium. This response results from the transfer of energy from plasma-generated species into the liquid phase through excitation-relaxation and ion-neutral collision processes at

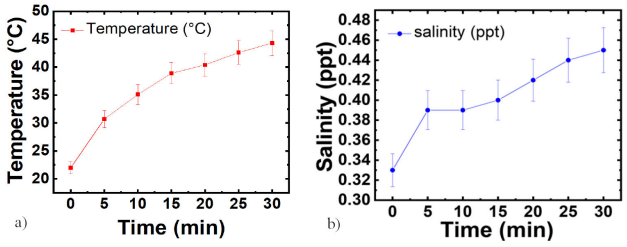


FIGURE 5. a) Bulk solution temperature and b) salinity as a function of plasma treatment time.

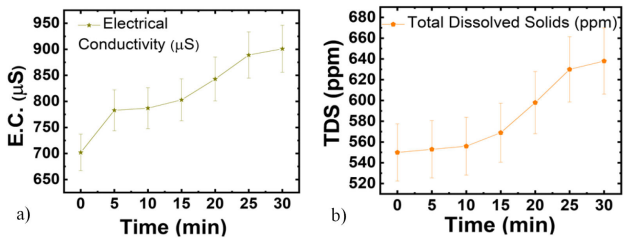


FIGURE 6. a) Electrical conductivity and b) total dissolved solids (TDS) as a function of plasma treatment time.

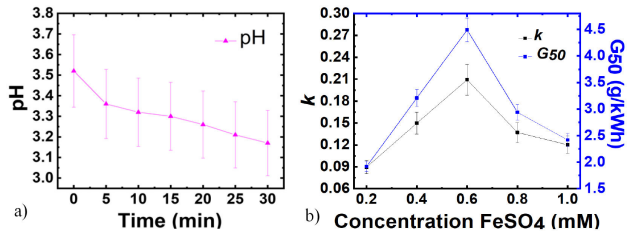


FIGURE 7. a) pH variation and b) rate constant (κ) and G_{50} as a function of $FeSO_4$ concentration.

the plasma-liquid interface [20]. Concurrently Salinity increased from approximately 0.33 to 0.45 ppt [Fig. 5b)], reflecting progressive accumulation of dissolved ionic species from oxidative fragmentation of AB9 and plasma-driven RONS formation, consistent with the initial stages of organic mineralization in AOPs systems [21].

Electrical conductivity increased from approximately 702 to 901 μS/cm [Fig. 6a)], driven by ionic species released during plasma-driven oxidative degradation of AB9. As the dye's aromatic structure is fragmented, ionic degradation products accumulate in solution, continuously feeding the conductivity increase throughout treatment [22]. TDS values increased from approximately 550 to 640 ppm [Fig. 6b)], closely paralleling the conductivity trend. Together, these parameters confirm ongoing mineralization: both increase as large organic structures are converted into low-molecular-weight ionic species [22].

Solution pH declined progressively from 3.52 to 3.17 [Fig. 7a)]. This acidification is primarily driven by the formation of HNO_3 and HNO_2 from gas-phase reactions between atmospheric nitrogen, water vapor, and plasma-generated species, supplemented by intermediate organic acids formed during AB9 fragmentation [19].

3.5. Energy efficiency: G_{50} parameter

A parameter for measuring energy efficiency in the degradation of pollutants is the G_{50}, which is defined as the amount of pollutant removed per unit of energy consumed to achieve 50% degradation [23,24]. The energy efficiency of the decolorization process was evaluated using the G_{50} parameter:

$$G_{50} = 1.8 \times 10^6 \frac{C_0 V_0 M}{P t_{50}}. \quad (6)$$

TABLE I. Comparison of G_{50} values for plasma-based degradation processes [24,25].

System	Contaminant	Catalyst / Conditions	G_{50}
NTAPP + $FeSO_4$ (this work)	Acid Blue 9	$FeSO_4$ (0.6 mM)	4.49
Non-thermal plasma	Acid Blue 25	Without catalyst	2.40
Dielectric Barrier Discharge (DBD)	Carbamazepine	Without catalyst	1.60
Dielectric Barrier Discharge (DBD)	2,4-Dinitrophenol	Without catalyst	0.94

For this study, $C_0 = 1.0 \times 10^{-4}$ M, $V_0 = 0.25$ L, $M = 792.86$ g/mol, and $P = 40$ W. The experimentally determined t_{50} values were 465, 277.8, 198.6, 303, and 268.4 s for 0.2, 0.4, 0.6, 0.8, and 1.0 mM $FeSO_4$, respectively, yielding G_{50} values of 1.92, 3.21, 4.49, 2.94, and 2.42 g/kWh [Fig. 7b)]. The maximum G_{50} of 4.49 g/kWh was achieved at 0.6 mM $FeSO_4$.

3.6. Comparative analysis of energy efficiency

Table I compares the G_{50} values obtained system achieves the highest energy efficiency among all entries listed, attributed to the synergistic interaction between plasma-generated RONS and the Fenton-type reaction at 0.6 mM $FeSO_4$ [24,25]. The availability of Fe^{2+} ions is sufficient to promote the decomposition of H_2O_2 generated by the plasma, increasing the production of ·OH radicals. At low concentrations (0.2 and 0.4 mM), the process is limited by insufficient catalyst availability, resulting in lower hydroxyl radical generation and a slower degradation rate. Conversely, at higher $FeSO_4$ concentrations (0.8 and 1.0 mM), the excess Fe^{2+} ions act as scavengers of ·OH radicals. This decreases the oxidative capacity and reduces the overall degradation efficiency.

3.7. Operating energy cost

Under optimal conditions (0.6 mM $FeSO_4$; $t_{1/2} = 198.6$ s; $P = 40$ W), the energy consumed to treat 250 mL was 0.00220 kWh. Applying CFE domestic electricity tariffs (0.987-3.218 MXN/kWh) [26], the estimated operating cost is 0.00217-0.00710 MXN per 250 mL, equivalent to 17.4-56.8 MXN/m^3 or approximately 0.50-1.64 USD/m^3.

From an operational standpoint, the energy cost analysis places the proposed system at 0.50-1.64 USD/m^3 under optimal conditions, which compares favorably with UV/H_2O_2, ozone-based, and photocatalytic systems reported in the literature. The reactor operates at atmospheric pressure, requires no chemical dosing beyond the catalytic $FeSO_4$ additive, and generates reactive species on demand without producing hazardous secondary byproducts. These characteristics collectively reduce the barriers to practical implementation, par-

TABLE II. Operating costs of the NTAPP + $FeSO_4$ system and other advanced oxidation processes reported in the literature [26-32].

Technology	Cost (USD/m^3)
NTAPP + $FeSO_4$ (0.6 mM)	0.50 – 1.64
UV/H_2O_2	∼5.80
O_3/H_2O_2	∼8.64
O_3/UV	up to 240
TiO_2/UV	4 – 12
Conventional ozone treatment	6 – 15

ticularly in decentralized or small-scale treatment contexts where reagent logistics and reactor complexity are limiting factors.

4. Conclusions

This study set out to evaluate whether $FeSO_4$ could meaningfully enhance the performance of a non-thermal atmospheric-pressure plasma system for degrading Acid Blue 9. The results confirm that it can but only within a narrow concentration window. At 0.6 mM $FeSO_4$, the system achieved near-complete decolorization and a mineralization efficiency exceeding 90% within 30 minutes, with a pseudo-first-order rate constant of $\kappa = 0.2093$ min^{-1} and an energy efficiency of $G_{50} = 4.49$ g/kWh. What these results demonstrate, more broadly, is that the combination of plasma-generated H_2O_2 and Fenton chemistry is not simply additive it is synergistic. Plasma alone produces RONS, but the integration of $FeSO_4$ converts a fraction of the accumulated H_2O_2 into additional ·OH radicals, extending the reactive lifetime of the system and enabling a level of mineralization that plasma alone, under the same power input and treatment time, would not achieve. The triarylmethane backbone of AB9 which confers both its chromophoric properties and its resistance to biological degradation is effectively dismantled under these conditions.

The broader implication is that NTAPP, when catalytically intensified, represents a technically sound and economically competitive option for the treatment of dye-contaminated wastewater. In a context where textile industry effluents continue to pose a documented risk to surface water quality and human health, and where freshwater scarcity makes wastewater reuse increasingly important, systems that achieve genuine mineralization, rather than phase transfer or partial decolorization, deserve serious consideration. The data reported here supports that case.

Acknowledgments

The authors wish to thank Herlinda Z. Pichardo Morales for technical support in the development of this work, as well as the following funding sources for their support: PRODEP DSA/103.5/15/6986, CA-5511-6/18-8304, and UAEMex 7440/2026CIB.

1. M. Berradi, R. Hsissou, M. Khudhair, M. Assouag, O. Cherkaoui, A. El Bachiri and A. El Harfi, Textile finishing dyes and their impact on aquatic environs, *Heliyon* **5** (2019) e02711, https://doi.org/10.1016/j.heliyon.2019.e02711
2. G. Kavitha, M. Govindhan, and S. Premkumar, Dye pollution and its implications for human health, aquatic ecosystems, and sustainable wastewater treatment: A comprehensive review, *J. Water Process Eng.* **80** (2025) 109071, https://doi.org/10.1016/j.jwpe.2025.109071
3. E. Forgacs, T. Cserhati, and G. Oros, Removal of synthetic dyes from wastewaters: A review, *Environ. Int.* **30** (2004) 953, https://doi.org/10.1016/j.envint.2004
4. T. Robinson and G. McMullan and R. Marchant and P. Nigam, Remediation of dyes in textile effluent: A critical review on current treatment technologies with a proposed alternative, *Bioresour. Technol.* **77** (2001) 247, https://doi.org/10.1016/s0960-8524(00)00080-8
5. S. Samsami and M. Mohamadizaniani and M. H. Sarrafzadeh and E. R. Rene and M. Firoozbahr, Recent advances in the treatment of dye-containing wastewater from textile industries: Overview and perspectives, *Process Saf. Environ. Prot.* **143** (2020) 138, https://doi.org/10.1016/j.psep.2020.05.034
6. H. Zollinger, Color chemistry: Syntheses, properties, and applications of organic dyes and pigments, 3rd ed. (Wiley-VCH, 2003), pp. 1-367.
7. M. A. Shannon and P. W. Bohn and M. Elimelech and J. G. Georgiadis and B. J. Mariñas and A. M. Mayes, Science and technology for water purification in the coming decades, *Nature* **452** (2008) 301, https://doi.org/10.1038/nature06599
8. V. Katheresan, J. Kansedo, and S. Y. Lau, Efficiency of various recent wastewater dye removal methods: A review, *J. Environ. Chem. Eng.* **6** (2018) 4676, https://doi.org/10.1016/j.jece.2018.06.060
9. J. A. Garrido-Cardenas and B. Esteban-García and A. Agüera and J. A. Sánchez-Pérez and F. Manzano-Agugliaro, Wastewater treatment by advanced oxidation processes and their worldwide research trends, *Int. J. Environ. Res. Public Health* **17** (2020) 170, https://doi.org/10.3390/ijerph17010170
10. Y. Deng and R. Zhao, Advanced oxidation processes (AOPs) in wastewater treatment, *Curr. Pollut. Rep.* **1** (2015) 167, https://doi.org/10.1007/s40726-015-0015-z

11. M. A. Oturan and J. J. Aaron, Advanced oxidation processes in water/wastewater treatment: Principles and applications. A review, *Crit. Rev. Environ. Sci. Technol*. **44** (2014) 2577, https://doi.org/10.1080/10643389.2013.829765

12. A. Barjasteh and Z. Dehghani and P. Lamichhane and N. Kaushik and E. H. Choi and N. K. Kaushik, Recent progress in applications of non-thermal plasma for water purification, *Appl. Sci*. **11** (2021) 3372, https://doi.org/10.3390/app11083372

13. P. Bruggeman and C. Leys, Non-thermal plasmas in and in contact with liquids, *J. Phys. D: Appl. Phys*. **42** (2009) 053001, https://doi.org/10.1088/0022-3727/42/5/053001

14. H. Zeghioud and P. Nguyen-Tri and L. Khezami and A. Amrane and A. A. Assadi, Review on discharge plasma for water treatment: Mechanism, reactor geometries, active species and combined processes, *J. Water Process Eng*. **38** (2020) 101664, https://doi.org/10.1016/j.jwpe.2020.101664

15. J. Sánchez, J. Beltrán, and M. T. Rodríguez, Removal of Erioglaucine (Acid Blue 9) with a new coagulant agent from Acacia mearnsii tannin extract, *Coloration Technol.* **128** (2012) 15, https://doi.org/10.1111/j.1478-4408.2011.00342.x

16. M. Flury and H. Flühler, Tracer characteristics of Brilliant Blue FCF, *Soil Sci. Soc. Am. J.* **59** (1995) 22, https://doi.org/10.2136/sssaj1995.03615995005900010003x

17. A. V. Borhade, D. R. Tope, and G. B. Dabhade, Removal of Erioglaucine dye from aqueous medium using ecofriendly synthesized ZnMnO3, e-J. *Surf. Sci. Nanotechnol*. **15** (2017) 74, https://doi.org/10.1380/ejssnt.2017.74

18. E. Brillas, I. Sirés, and M. A. Oturan, Electro-Fenton process and related electrochemical technologies based on Fenton's reaction chemistry, *Chem. Rev.* **109** (2009) 6570, https://doi.org/10.1021/cr900136g

19. J. J. Pignatello, E. Oliveros, and A. MacKay, Advanced oxidation processes for organic contaminant destruction based on the Fenton reaction and related chemistry, *Crit. Rev. Environ. Sci. Technol*. **36** (2006) 1, https://doi.org/10.1080/10643380500326564

20. A. Fridman, Plasma chemistry (Cambridge University Press, 2008), https://doi.org/10.1017/cbo9780511546075

21. H. Ghodbane and A. Y. Nikiforov and O. Hamdaoui and P. Surmont and F. Lynen and G. Willems and C. Leys, Non-thermal plasma degradation of anthraquinonic dye in water: Oxidation pathways and effect of natural matrices, *J. Adv. Oxid. Technol*. **17** (2014) 372, https://doi.org/10.1515/jaots-2014-0223

22. A. Babuponnusami and K. Muthukumar, A review on Fenton and improvements to the Fenton process for wastewater treatment, *J. Environ. Chem. Eng*. **2** (2014) 557, https://doi.org/10.1016/j.jece.2013.10.011

23. M. Rahimpour and M. Rahimpour and H. Taghvaei and S. Zafarnak and M. R. Rahimpour and M. R. Rahimpour and S. Raeissi, Post-discharge DBD plasma treatment for degradation of organic dye in water: A comparison with different plasma operation methods, *J. Environ. Chem. Eng*. **7** (2019) 103220, https://doi.org/10.1016/j.jece.2019.103220

24. M. A. Malik, Water purification by plasmas: Which reactors are most energy efficient?, *Plasma Chem. Plasma Process.* **30** (2009) 21, https://doi.org/10.1007/s11090-009-9202-2

25. Y. Cao and G. Qu and T. Li and N. Jiang and T. Wang, Review on reactive species in water treatment using electrical discharge plasma: Formation, measurement, mechanisms and mass transfer, P*lasma Sci. Technol*. **20** (2018) 103001, https://doi.org/10.1088/2058-6272/aacff4

26. CalcUle MX, Precio kWh CFE 2026: Tarifas 1, 1B, 1C, DAC y Recibo, https://www.calcule.com/guias/cfe/ tarifas-electricas/ (2026).

27. Y. Zhang and K. Shaad and D. Vollmer and C. Ma, Treatment of textile wastewater using advanced oxidation processes-A critical review, *Water* **13** (2021) 3515, https://doi.org/10.3390/w13243515

28. N. Azbar, T. Yonar, and K. Kestioglu, Comparison of various advanced oxidation processes and chemical treatment methods for COD and color removal from a polyester and acetate fiber dyeing effluent, *Chemosphere* **55** (2003) 35, https://doi.org/10.1016/j.chemosphere.2003.10.046

29. S. Mehdizadeh and S. Sadjadi and S. J. Ahmadi and M. Outokesh, Removal of heavy metals from aqueous solution using platinum nanoparticles/Zeolite-4A, *J. Environ. Health Sci. Eng.* **12** (2014) 7, https://doi.org/10.1186/2052-336x-12-7

30. E. N. Kadioglu and H. A. Eroglu and H. Ozturk and F. Akbal and A. Kuleyin, Enhanced degradation of textile wastewater by activated carbon-assisted Fenton oxidation: Economic analysis and ANN-based optimization, *Biomass Conv. Bioref.* **15** (2025) 17775, https://doi.org/10.1007/s13399-025-06599-1

31. M. N. Chong and B. Jin and C. W. Chow and C. Saint, Recent developments in photocatalytic water treatment technology: A review, *Water Res*. **44** (2010) 2997, https://doi.org/10.1016/j.watres.2010.02.039

32. K. Ikehata and M. G. El-Din, Aqueous pesticide degradation by ozonation and ozone-based advanced oxidation processes: A review (Part I), *Ozone: Sci. Eng*. **27** (2005) 83, https://doi.org/10.1080/01919510590925220